THESIS

ADDRESSING LOW-COST METHANE SENSOR CALIBRATION SHORTCOMINGS WITH MACHINE LEARNING

Submitted by

Elijah Kiplimo

Department of Systems Engineering

In partial fulfillment of the requirements

For the Degree of Master of Science

Colorado State University

Fort Collins, Colorado

Spring 2025

Master's Committee:

Advisor: Bryan Rainwater
Co-Advisor: Daniel J. Zimmerle

Thomas Bradley
Nazemi Reza
Stuart Riddick

ABSTRACT

ADDRESSING LOW-COST METHANE SENSOR CALIBRATION SHORTCOMINGS WITH MACHINE LEARNING

Quantifying methane emissions is essential for meeting near-term climate goals and is typically done using methane concentrations measured downwind of the source. One major source of methane important to observe and remediate is fugitive emissions from oil and gas productions sites; however, installing methane sensors at thousands of sites within a production basin can be prohibitively expensive. In recent years, relatively inexpensive metal oxide sensors have been used to measure methane concentrations at production sites. Current methods used to calibrate metal oxide sensors have been shown to have significant shortcomings, resulting in limited confidence in methane concentrations generated by these sensors. To address this, we investigate using a machine learning (ML) model to convert metal oxide sensor output to methane mixing ratios. To generate data to train this model, two metal oxide sensors, TGS2600 and TGS2611, were collocated with a trace methane analyzer downwind of controlled methane releases. A comparison of histograms generated using the analyzer and metal oxide sensors mixing ratios show overlap coefficients of 0.95 and 0.94 for the TGS2600 and TGS2611, respectively. Overall, our results showed there was good agreement between the ML derived metal oxide sensors' mixing ratios and those generated using the more accurate trace gas analyzer. This suggests that the

response of lower-cost sensors calibrated using ML could be used to generate mixing ratios with higher precision and accuracy, thereby reducing the cost of sensor deployments, and allowing for timely and accurate tracking of methane emissions.

Keywords: Methane; quantification; metal-oxide; sensor; calibration; machine learning.

ACKNOWLEDGEMENTS

Prof Daniel Zimmerle: Thank you for offering me the opportunity to work at METEC and study at CSU.

Dr Bryan Rainwater: Thank you for your unwavering support and guidance throughout my journey. Your mentorship has been instrumental in shaping me into a skilled software engineer and a critical thinker. Thank you for your encouragement, insights, and for fostering my overall growth and development.

Prof Thomas Bradley: Thank you for bringing part of my committee and for your support through my master's in systems engineering.

Dr. Nazemi Reza: Thank you for being part of my thesis committee and for your valuable insights into this project.

Dr. Stuart Riddick: I sincerely appreciate Dr. Stuart's guidance throughout this project, from assisting with experiment setup and data collection to providing continuous feedback. Thank you for your support in developing this publication and for your invaluable insights into the methane field and the METEC group.

METEC Group: Thank you to the entire METEC team for the constant feedback through this project. I specially thank Ryan Bouwer, Mercy Mbua and Dan Fleischmann for your support in the setup and development of this project.

DEDICATION

I dedicate this work to my family: My wife Mercy, The Koech's (Paul & Clementine Koech, Beatrice, Isaac, Rebecca, Victor, Faith and Grace). Thank you for your belief in me.

TABLE OF CONTENTS

LIST OF FIGURES

1. INTRODUCTION

Methane (CH_4), a gas with a global warming potential 25 times greater than carbon dioxide, has increased in atmospheric composition by a factor of three since preindustrial times largely due to changes in emissions from anthropogenic activities [1,2]. Nearly all countries have entered into treaties or agreements to reduce methane emissions; however, it has recently been suggested that methods used to quantify methane emissions are insufficiently precise to measure emissions reduction from mitigation strategies [3–6]. Since the 1990s, numerous studies have focused on measuring methane emissions from oil and gas production activities, highlighting their environmental impact and the need for accurate monitoring[7–12].

Methane monitoring is not only critical for oil and gas operations but also for understanding emissions from a wide range of sources, including agriculture, waste, and urban activities. The complexity of methane emissions is further compounded by the variability in emission profiles across different basins and facility types. For example, in the Denver-Julesburg Basin (DJ Basin), methane emissions from oil and gas operations are intermixed with emissions from agricultural and urban sources, making accurate attribution and quantification particularly challenging. This complexity underscores the need for robust monitoring systems that can adapt to diverse environments and provide reliable data for emissions inventories.

Measurement approaches have evolved from survey-based methods, which utilize instruments mounted on mobile platforms for short-duration measurements [13–15], to continuous monitoring techniques, where fixed-location instrumentation enables long-term data collection [6,16–18].

The advantage of continuous monitors is that observations are more likely to detect the short-duration, large-emission events that are typical of oil and gas emission distributions and are essential to capture if realistic emissions estimates are to be generated [19,20]. Typically, on-site continuous monitoring systems include several (minimum of four) stationary methane measurement/meteorological instrumentation packages installed around a site and coupled with a dispersion model to infer a rate of emission [6,21,22]. One difficulty in designing a continuous monitoring system for an oil and gas production site is the choice of methane measurement instrumentation, varying significantly in cost and performance.

Examples of methane sensing technologies and costs can include, but are not limited to, metal oxide sensors ($1 - $15 per sensor), integrated infrared sensors ($100 - $300 per sensor), and tunable diode laser absorption spectrometers and other optical cavity-based instrumentation ($500 - $50,000 per sensor). As there are thousands of productions sites across the US alone, costly methane measurement systems can be prohibitively expensive to deploy at every site; therefore, metal oxide sensors are increasingly being widely deployed across oil and gas production sites across the US [6,22].

As metal oxide sensors are being widely distributed to measure near-background methane concentrations in air (typically below 100 ppm), many studies have described methods of

calibration, deployment, and response, however, these sensors are sensitive to temperature and relative humidity and require individual calibration [17,23–30]. Typical metal oxide sensors used include the Taguchi Gas Sensors (TGS) 2600 and 2611 models produced by Figaro Engineering Inc. (Osaka, Japan). TGS2600 uses a tin-dioxide (SnO_2) sensing layer that reacts with the detected gases. The detection mechanism relies on the change in electrical conductivity through the SnO_2 in the presence of methane. Adsorption of oxygen molecules occurs on the surface of SnO_2 forming O^{2-} ions leading to electron capture that creates a depletion layer at the surface of the SnO_2 and increases its resistance [23,24]. Methane interacts with the adsorbed oxygen ions releasing the trapped electrons back into the SnO_2 conduction band, decreasing its resistance. The change in resistance is proportional to the concentration of CH_4. The TGS2611 has the same operation basis as the TGS2600 but has been optimized for methane detection by the integration of a filter material that selectively permits methane to reach the sensing element while blocking other gases [23,24]. Studies using Figaro TGS sensors have measured the resistance change across the metal oxide strip to infer changes in concentration. It is assumed the metal oxide sensor has relatively constant resistance in clean air (R_0, Ω) and becomes lower in the presence of methane (R_s, Ω). The ratio of these resistances gives a measure of the methane mixing ratio in air. The resistance of the metal oxide sensor is also affected by the air temperature (T_a, °C) and relative humidity (rH, %), and the ratio of resistance can be corrected to account for these factors using an empirically derived algorithm (Equation (1)) [25].

$$\left(\frac{R_s}{R_0}\right)_{corr} = \frac{R_s}{R_0}.(0.024 + 0.0072.rH + 0.0246.T_a) \quad (1)$$

The temperature and humidity corrected ratio of R_s and R_0 is then typically converted to a methane mixing ratio using a sensor-specific calibration algorithm [25,30]. As they perform poorly in low relative humidity, at less than 40% RH [30], the TGS sensors are typically calibrated by comparing $(R_s/R_0)_{corr}$ to methane mixing ratios measured using a sub-ppm reference instrument measuring methane contemporaneously. An algorithm is then generated to translate $(R_s/R_0)_{corr}$ to a calibrated mixing ratio ($[CH_4]_{cal}$). Published algorithms have commonly used linear, power, and/or exponential functions to generate mixing ratios on a per-sensor basis [17,23,25,26,30,31]; however, there is not an accepted understanding of differences between individual sensors' response to changing methane concentrations beyond differences in manufacturing [17].

Within the calibrated methane mixing ratio there are several potential sources of uncertainty:

1. The measured resistance (R_s) appears to be highly variable between individual sensors. Through trial and error, the output of some sensors in near background mixing ratios (< 10 ppm) can become almost indistinguishable from the noise.
2. The calculation of $[CH_4]_{cal}$ is heavily dependent on determining a value for the TGS resistance in clean air, R_0.
3. Given the variability in response of sensors to changes in methane concentration, sensors will also likely respond variably to changes in relative humidity and temperature (as defined in Equation 1).

Overall, these uncertainties raise concerns about the historical methods for calibrated TGS sensor methane mixing ratios.

An alternative approach is to use machine learning to account for low signal to noise ratios and differences in sensor response to relative humidity and temperature variation. Recent developments in machine learning algorithms have transformed sensor calibration and enhanced their reliability in environmental monitoring [32]. One example of machine learning is the Random Forest (RF) Regressor developed by Leo Breiman in 2001. Random Forest is an ensemble machine learning model [35], built upon the combination of predictions from multiple simpler models[33]. Random Forest uses a collection of decision trees that split the data into branches based on the input features to make a prediction. Training the RF regression model involves presenting the model with the input variables (metal oxide sensors' resistances, temperature and relative humidity) that are passed through multiple decision trees and the output aggregation predict the target variable (in this case the trace gas analyzer CH_4 concentrations).

The calibration of low-cost metal oxide sensors, as explored in this study, is a critical step toward enabling widespread deployment of continuous methane monitoring systems. However, the challenges associated with sensor variability, environmental sensitivity, and low signal-to-noise ratios must be addressed to ensure the reliability of these systems. The Random Forest (RF) machine learning approach proposed here offers a promising solution by leveraging the ability of machine learning to model complex, non-linear relationships between sensor inputs and methane concentrations. This approach not only improves calibration accuracy but also provides a

framework for integrating data from multiple sensors and environmental variables, making it highly applicable to large-scale deployments.

Beyond this study, broader research has focused on advancing methane monitoring technologies and methodologies to support emissions mitigation efforts. For instance, the Site Aerial Basin Emissions Reconciliation (SABER) project demonstrated how high-frequency sampling and mechanistic modeling can improve emissions inventories, while driving surveys provided valuable insights into the spatial and temporal variability of methane emissions. These experiences have informed the development of the RF-based calibration approach, highlighting the importance of combining field measurements with advanced data analysis techniques. Moving forward, the integration of low-cost sensors with machine learning algorithms has the potential to revolutionize methane monitoring by providing cost-effective, accurate, and scalable solutions for emissions quantification. This work contributes to the growing body of research aimed at addressing the global challenge of methane emissions and supports the development of policies and technologies for climate change mitigation.

We propose a method using two TGS sensors to report on the RF machine learning approach for generating calibrated methane mixing ratios. Specifically, we will

1) Collect R_s values from low-response TGS2600 and TGS2611 sensors contemporaneously with a sub-ppm methane analyzer.
2) Generate calibrations curves using (a) the traditional method (presented above) and (b) RF machine learning approach.

3) Compare the calibrated methane mixing ratios reported by the TGS2600 and TGS2611 to the methane analyzer to generate an understanding of sensor type response, bias and drift over time. Ultimately, we aim to provide evidence to understand if the RF machine learning approach can generate better calibration algorithms than currently used methods.

2. MATERIALS AND METHODS

2.1 Methane measurement

2.1.1 Figaro TGS sensors

Both the TGS 2600 and 2611 sensors were connected to a Raspberry Pi 4 (London, UK) via an ADS1115 16-Bit analog to digital converter, in near proximity to a DHT22 temperature and humidity sensor. The sensors were powered by the Raspberry Pi's MaxLinear MxL7704 regulator. The TGS 2600, 2611 and DHT22 were connected to the A0, A1 and A2 pin of the module, respectively. Figure 1 illustrates the system architecture, providing an overview of its structure and components. A python script was used for continuous reading of data at 1s intervals. The script leveraged the Inter-Integrated Circuit (I2C) communication protocol to interface with the ADS1115, deploying the Adafruit ADS1x15 library for data acquisition. The acquired data was timestamped and written to daily files.

The ADS1115 16-bit analog-to-digital converter (ADC) was used to interface the TGS sensors with the Raspberry Pi. The ADS1115 was selected for its high resolution and low noise, which is critical for accurately measuring the small resistance changes in the TGS sensors. To ensure stability across varying temperatures, the ADS1115 was operated within its specified temperature range (-40°C to +125°C), and its internal temperature compensation circuitry minimizes drift. Additionally, the ADC readings were periodically validated against known reference voltages to confirm stability. The temperature correlation for the TGS2600 and TGS2611 sensors was found

to be minimal (0.26 and -0.28, respectively), indicating that the ADS1115 maintained consistent performance throughout the experiment, even under varying environmental conditions

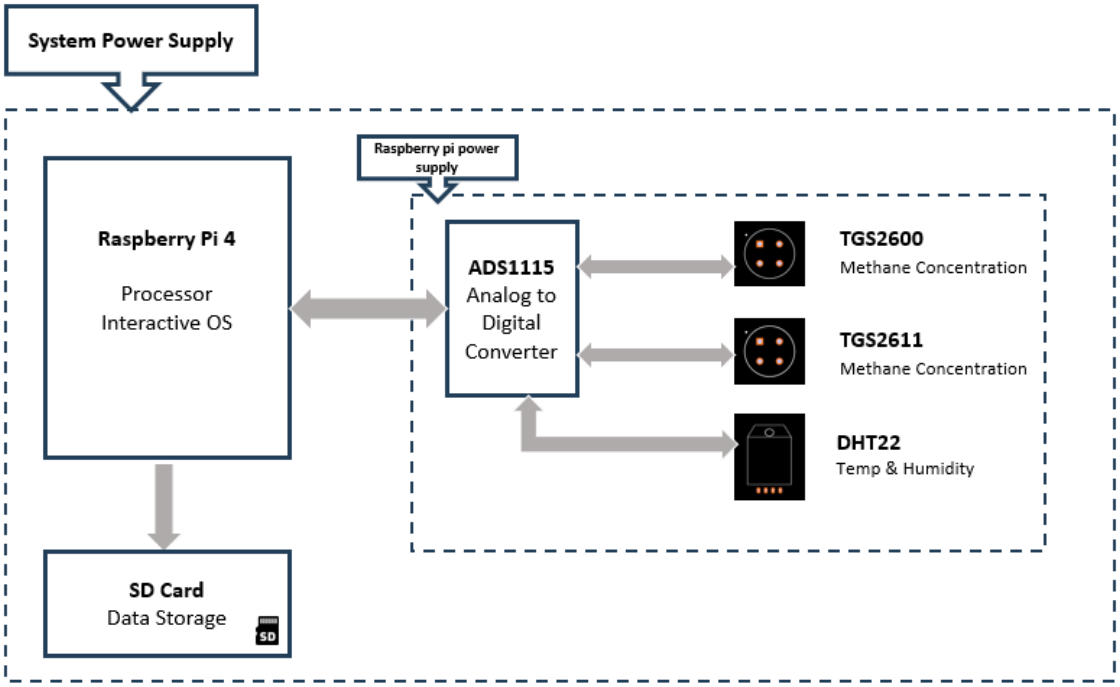

Figure 1: System architecture of sensor integration, power supply and data acquisition

2.1.2 Reference instrument – Aeris MIRA Ultra Mobile LDS

The Aeris Technologies, Inc. (Hayward, CA, USA) Ultra is a mid-infrared laser absorption analyzer [34]. This instrument achieves simultaneous quantification of methane between 10 ppb and 10,000 ppm, and ethane between 1 ppb and 1,000 ppm. [34]. The device operates at standard rates of 1 or 2 Hz, with an option to increase it to 10 Hz. For these experiments, the instrument was set to measure at 5Hz.

2.2 Controlled methane release experiments

Between 1st March 2024 and 2nd May 2024, controlled methane release experiments were conducted at Colorado State University's Methane Emission Technology Evaluation Center (METEC) in Fort Collins, Colorado. The experiments simulated real-world oil and gas production emissions by releasing natural gas of a known composition from multiple infrastructure points, including wellheads, separators, and tanks. The releases took place at multiple sites (pads 4 and 5) with emissions ranging from 0.005 to 8 kg of methane per hour (CH_4 h^{-1}). The methane releases were both single and multi-source, imitating specific operational scenarios and emissions patterns (Figure 2).

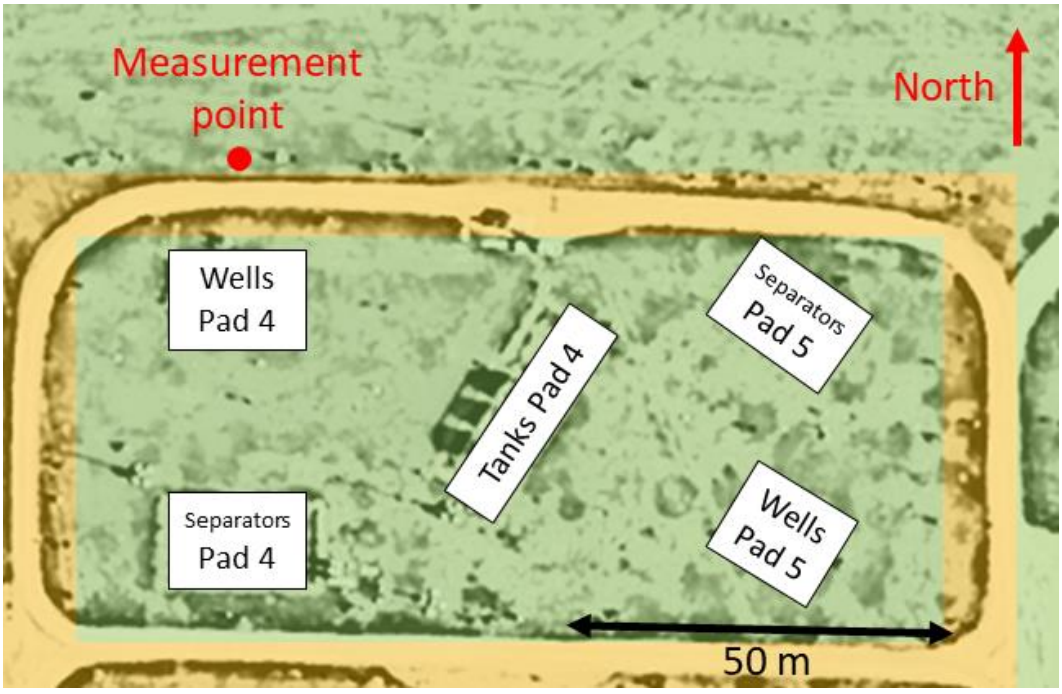

Figure 2: Field layout of the METEC site in Fort Collins with the measurement location on the north of the site

Throughout the study, the TGS methane sensors and the inlet of the Aeris Sentinel analyzer were located at the north-western part of the facility (approximately 40.60° N, 105.14° W) at a height of two meters above the ground. The inlets of the TGS methane sensors and the Aeris were collocated to ensure simultaneous sampling of the same air mass (Figure 3). This configuration minimized spatial variability and ensured data from both systems were temporally aligned, allowing for direct comparison between the TGS sensor outputs and the reference methane concentration. The experimental period spanned a broad range of environmental conditions, with external temperatures varying significantly from -22 °C earlier in the year to +30°C towards the end of the deployment.

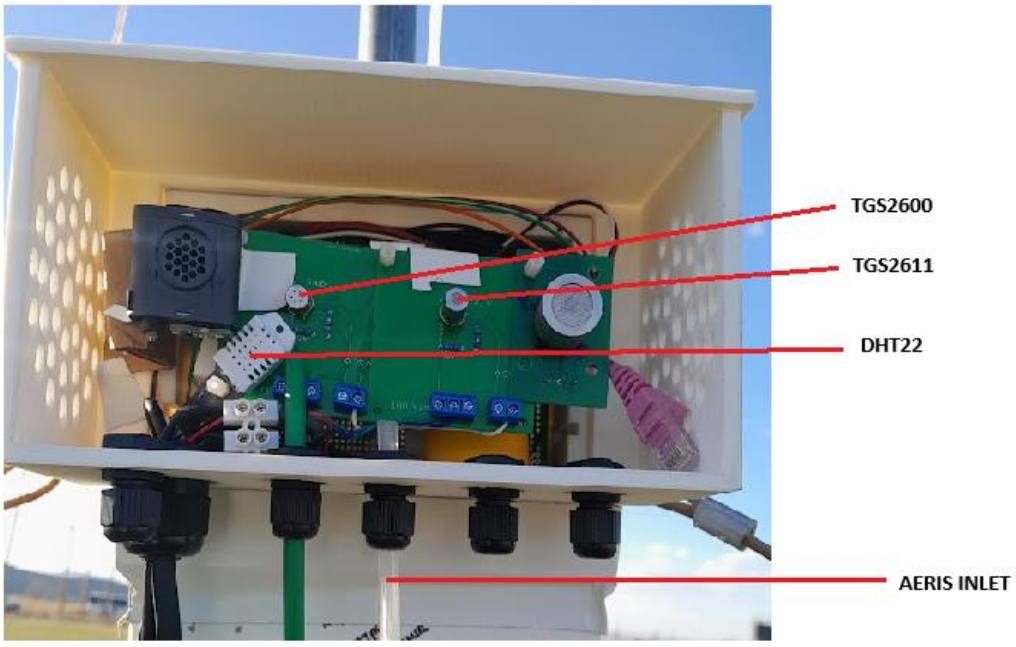

Figure 3: Experimental sampling setup for TGS2600, TGS2611, DHT22 and Aeris Sentinel

The two sensors were investigated for their resistance in clean air to evaluate stability in comparison the reference analyzer (background of 1.8 – 2.1ppm), and each TGS sensor was measured and normalized. The TGS2600 and TGS2611 sensors raw readings from the 16-bit analogue to digital converter reported an average of 29076.85 and 4714.29 within the baseline to air range. Within this range, TGS2600 had mean deviations of -65.59 indicating that the sensor resistance was slightly lower than baseline to clean air while the TGS2611 with a deviation of 88.60 had readings that were slightly higher than the average clean air resistance. The temperature correlation for TGS2600 and TGS2611 was 0.26 and -0.28 respectively, indicating minimal effect of temperature on the baseline resistance. Humidity had a negligible correlation for TGS2600 (-0.02) while TGS2611 showed a positive correlation of 0.17 with humidity. In both instances, the correlations were weak and therefore there was no need to compensate for the effects at baseline resistance. The signal-to-noise ratio (SNR) for the TGS2600 and TGS2611 sensors were calculated from empirical data to assess the quality of the sensor signals. SNR was determined using the formula:

$$SNR(dB) = \log_{10}(\frac{P_{signal}}{P_{noise}})$$

where P_{signal} is the power of the noise (calculated as the variance of the sensor resistance in the absence of methane) and P_{noise} is the power of the noise (calculated as the variance of the sensor resistance in the absence of methane). The TGS2600 exhibited an SNR of 26.98 dB, while the TGS2611 exhibited an SNR of 21.24 dB. These values indicate strong signal quality and minimal noise interference, which is critical for accurate methane concentration measurements. The higher

SNR of the TGS2600 suggests that it is slightly more robust to noise compared to the TGS2611, which aligns with its slightly better performance in low-concentration environments. These results indicate strong signal quality and minimal noise interference for both sensors when operating in clean air conditions at relatively constant temperature and humidity.

2.3 Eugster and Kling (2012) metal oxide sensor calibration

A calibration following published methods [25,30] was performed on a subset of the TGS2600 and TGS2611 data collected during the controlled release experiments. After calculating the resistance of the metal oxide sensor, this resistance (R_s) was then normalized against the resistance of the sensor in background methane (R_0), and then corrected for temperature and relative humidity (Equation (1)). The $(R_s/R_0)_{corr}$ was plotted against a subset of the contemporaneous methane mixing ratios measured by the Aeris sentinel to generate a calibration algorithm. This algorithm was then used to generate calibrated mixing ratios ($[CH_4]_{cal}$) for every measurement.

2.4 Machine learning calibration

2.4.1 Data Preprocessing

In this study, the Random Forest (RF) algorithm was used to predict methane concentrations from the TGS sensor outputs, and temperature and relative humidity measured by the DHT22. In the RF algorithm, grouped decision trees act as flowcharts where the internal nodes represent decisions made on features and branches representing the decision outcome, with the leaf nodes being the final prediction (Figure 4). The first step in RF is the creation of subsets of the original dataset,

where data are drawn with replacement from the original dataset. This approach reduces overfitting by enabling each tree to be created with different subsets of data and minimizes the correlation between the trees without increasing the variance[33]. The second stage randomly selects a subset of features to construct decision trees. This ensures diverse trees as not all trees make the same splits and thus prevents similarity between trees. By generating a diverse and uncorrelated group of trees, this process helps to minimize predictive errors, ultimately producing a stronger and more reliable final prediction. To make a prediction, the individual tree outputs are aggregated and hence a prediction is made.

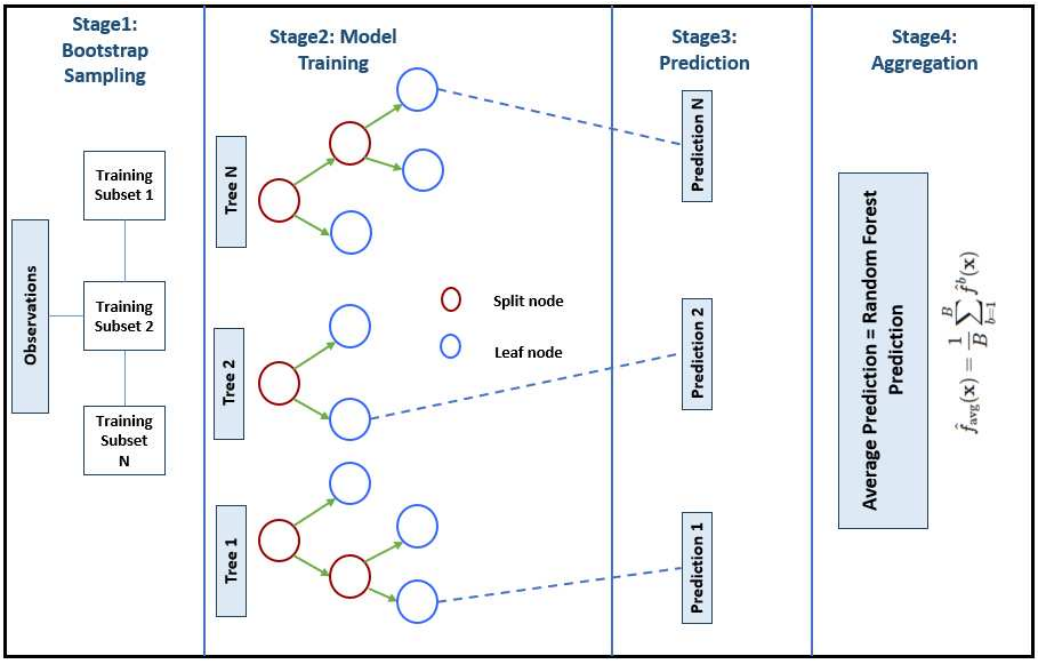

Figure 4: Graphical Representation of Random Forest (RF) regression process

The data from the two methane sensors and the DHT22 were then compiled in one file. Since the data was collected synchronously from all sensors, each timestamp corresponded to a consistent

set of sensor readings. The data gathering script also ensured that all sensor signals were received before being written to the main file, while introducing delays in cases where the DHT22 sensor signals were not received. This approach guaranteed the completeness of the datasets.

While a total of 1.6 million raw datapoints were collected during the study, multiple factors led to reduction in the data set used for this study. There were instances of power loss and high winds tipping our data collection mast, necessitating 48-hour preheating periods for the sensors each time this occurred [35]. Furthermore, during our analysis, there were instances of high emissions, and we corrected for the sensor time constants ensuring that the sensors was fully flushed before the next reading. These factors combined led to elimination of 424,000 data points. Consequently, our model was trained and tested on 518,168 datapoints, roughly 44% of the overall dataset. The datasets used in our model training aligns with recommendations, with tens of thousands of points generally sufficient to achieve reliable and accurate results [33,36].

To align the temporal resolution of the Aeris MIRA Ultra analyzer (sampled at 5 Hz) with the slower-responding TGS2600 and TGS2611 sensors, the data was averaged over 60-second intervals. A moving average filter was applied to the Aeris MIRA data to smooth high-frequency noise and synchronize the datasets for calibration and machine learning model training.

The frequency response of the TGS sensors was modeled as a first-order system with a time constant (τ), where the response to a step input x(t) is given by:

$$y(t) = x(t).\left(1 - e^{-\frac{1}{\tau}}\right)$$

The time constants for the TGS2600 and TGS2611, approximately 60 seconds as specified by the manufacturer, were used for data averaging. To account for the slow response, a low-pass filter was applied to the Aeris MIRA data, with a cutoff frequency of $f_c=\frac{1}{2\pi\tau}$ where τ is the time constant of the sensors. Figure 5 illustrates the scaled and time-aligned responses of the TGS2600, TGS2611, and Aeris sensors after applying these adjustments.

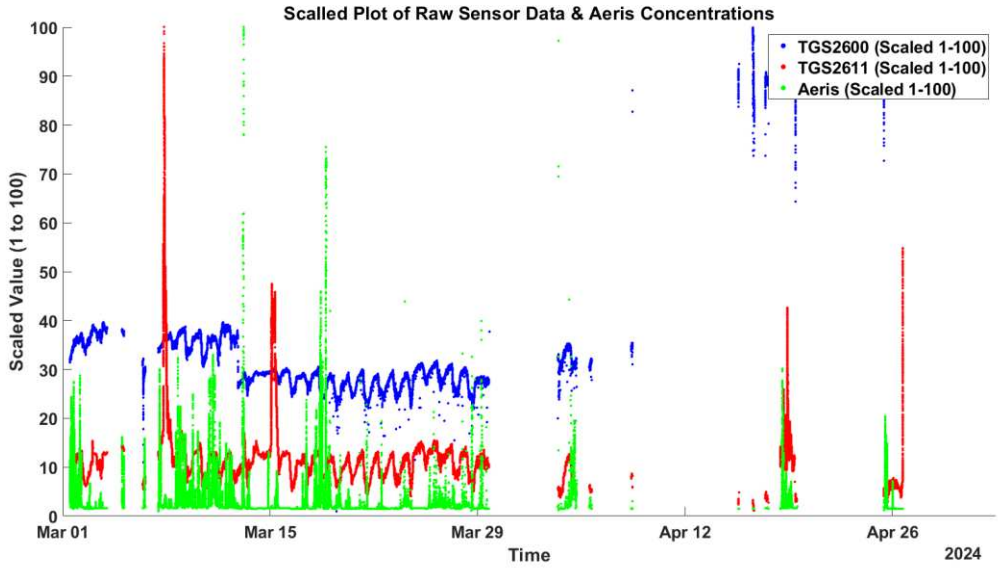

Figure 5: Scaled and time-aligned responses of the TGS2600, TGS2611, and Aeris sensors after applying a moving average filter to account for the sensors' frequency response

2.4.2 Model Training

Google Colab environment was used for training, saving and making predictions using the model. This environment provided an ideal Graphical Processing Unit (GPU) to efficiently handle the dataset and run the Random Forest Regressor model. Within the environment, pandas library was used for data manipulation and analysis, Scikit-Lean library for machine learning tools, Joblib library for object serialization and matplotlib for visualizations. The RF model input data was split

into training and testing using 70-30 criteria, and the split was done randomly to eliminate bias and ensure a meaningful representation of the data distribution.

Denoting the original dataset as D with N observations, each sample x_i has a probability $\frac{1}{N}$ of being selected each time and the sample can be selected several times (Equation 2).

$$D= \{x_1, x_2, \ldots\ldots, x_N\} \quad (2)$$

The bootstrapped dataset, D^*, is expressed as a function of each bootstrapped sample, x_i*, drawn independently from D with replacement (Equation 3).

$$D^*=\{x_1^*, x_2^*, \ldots, x_N^*\} \quad (3)$$

There were three input features to the model and the maximum features hyperparameter of three was defined in the code. Previous studies show that the near optimum results are given by the square root of the total number of features [35], but in our case we used all features to create the trees as there were a smaller number of features. The created trees enhance the model's predictive performance by reducing the variances through the creation of child nodes (Figure 4) that are more homogeneous with respect to the target variable.

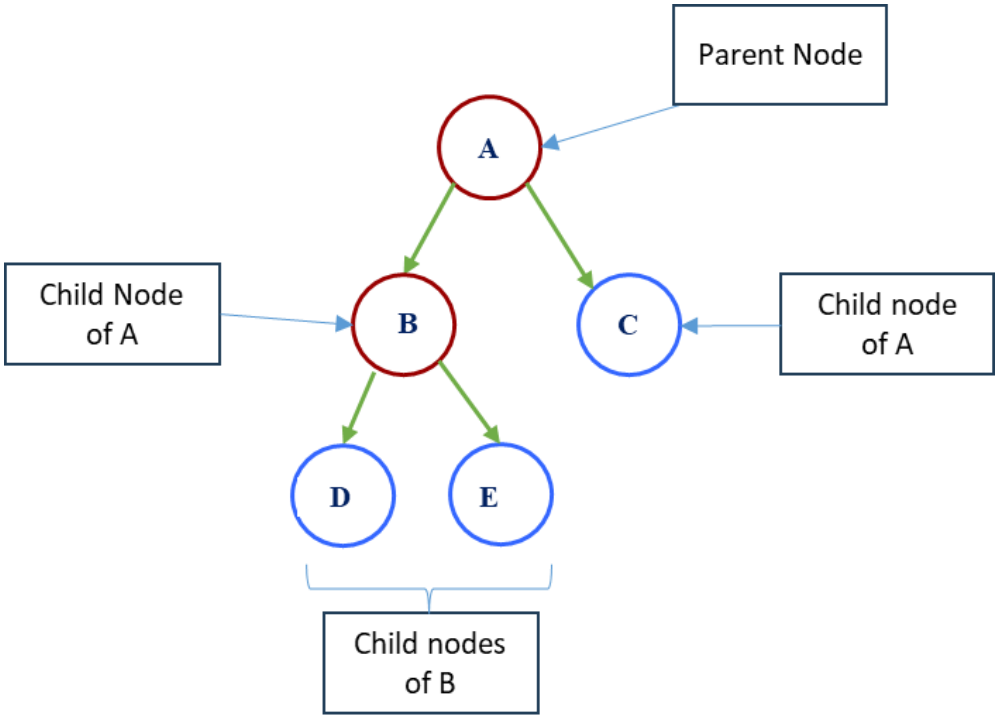

Figure 6: RF Tree structure

The variance of each observation (V_y) is calculated from each concentration observed by the Aeris analyser (y_i), the total number of observations (n), and the mean of the observed values (y^*, Equation 4).

$$V_y = \frac{1}{n}\sum_{i=1}^{n}(y_i - y^*)^2 \qquad (4)$$

Once the values are split into child nodes based on the features, each of the tree nodes (left and right) has an associated variance. The aim of tree splitting is to minimize the overall variance, and this is achieved by evaluating the reduction in variance (V_r) achieved through the comparison of parent node variance (P_{Vy}) to the weighted average of the child nodes' variance for the total number of observations in the parent node (n; Equation 5). The weighted average of the child nodes'

variance is calculated from the number of measurements in the left (n_l) and right (n_r) nodes and the variance of the measurements in the left (V_{yl}) and right (V_{yr}) nodes.

$$V_r = P_{v_y} - \left(\left(\frac{n_l}{n}\, x\, V_{y_l}\right) + \left(\frac{n_r}{n}\, x\, V_{y_l}\right)\right) \qquad (5)$$

The final prediction of the RF regressor model was determined through the aggregation of the predictions from individual trees in the forest. K-fold cross validation was employed to evaluate the performance of the RF models for the two sensors. Due to the limited available computing resources, a stratified k-fold approach with 5 folds was used, providing a reliable estimate of the model performance. The trained random forest regressor model was stored and used to calculate mixing ratios based on the metal oxide and DHT22 temperature and humidity outputs.

2.4.3 Model Evaluation Metrics

Methane mixing ratios calculated using the ML approach were compared to mixing ratios measured by the Aeris Ultra analyzer output using the coefficient of determination (R^2) of the linear regression between the data, the mean absolute error (MAE), the mean squared error (MSE), the root mean squared error (RMSE) and the mean absolute percentage error (MAPE) . The feature importance, which is the measure of how each input variable contributes to the model prediction, was also evaluated for the ML calculated data. Feature importance is determined by evaluating the reduction in impurity (measure of how mixed or uncertain the target variable is within a node) at each node, regulated by the probability of reaching that node [37]. Histograms of measured and modelled mixing ratio data, comprising of 0.2 ppm bins truncated at < 2ppm and >5 ppm, were compared using the overlap coefficient to investigate the overlap of data.

3. RESULTS

The percentage error analysis for methane (CH_4) concentration measurements using the TGS2611 and TGS2600 sensors (Figure 6) indicates that the majority of data points fall within the 10% error range, with TGS2600 achieving slightly higher accuracy than TGS2611. Specifically, 29.9% of the TGS2600 measurements were within 10% error, compared to 28.9% for TGS2611. Both sensors exhibited a low proportion of high-error measurements, with less than 1% of data points exceeding 50% error. Throughout the experiment, the temperature varied with large diurnal cycles from a maximum of 30 °C to a minimum of -22 °C with relative humidity cycling similarly between a maximum of 100% and minimum of 18%.

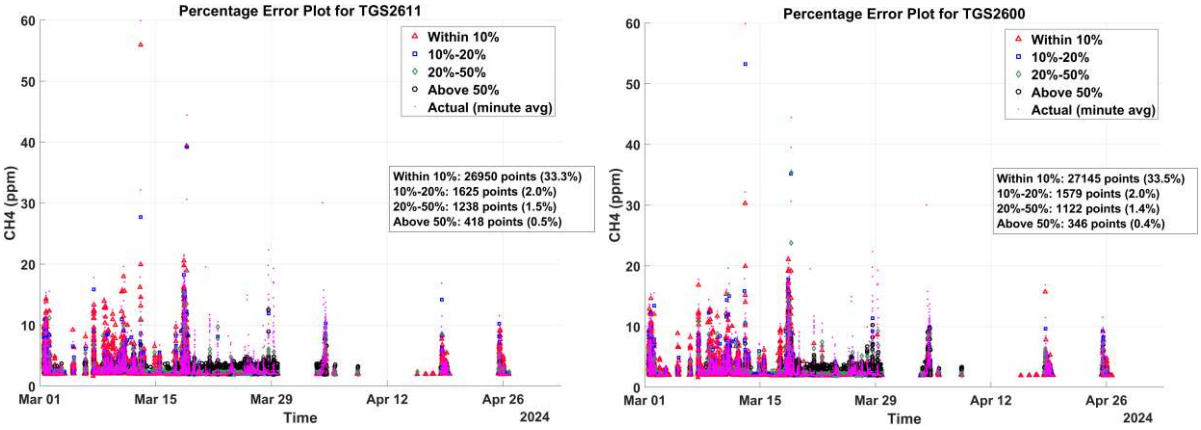

Figure 7: Percentage error plots for methane (CH_4) concentration measurements using (left) TGS2611 and (right) TGS2600 sensors. The error distribution is categorized into four ranges: within 10% (red triangles), 10%-20% (blue squares), 20%-50% (green diamonds), and above 50% (black circles). The actual minute-averaged CH_4 concentrations are shown in magenta. Most data points for both sensors fall within the 10% error range, with TGS2600 exhibiting a slightly higher percentage of accurate measurements compared to TGS2611

3.1 Eugster and Kling (2012) calibration method

3.1.1 Calibration curves

Previous studies describing the use of metal oxide sensors to measure methane concentrations in air have reported either linear or exponential relationships between $(R_s/R_0)_{corr}$ and methane mixing ratios measured by a trace methane analyzer [17,23–26,30,31,38]. Unlike these studies, the TGS sensors used in this study did not respond in the same way and there was no discernible relationship between $(R_s/R_0)_{corr}$ and methane mixing ratio with R^2 of 0.0015 and 0.0015 for the TGS2600 and TGS2611, respectively (Figure 7).

It was later discovered that the TGS sensors used in this study produced a much lower signal-to-noise ratio compared to other studies [25,30]. As a result, the data reported by these sensors could not be calibrated using the methods described in previous research. When the linear calibration algorithms were used to calculate the methane mixing ratio and compared against the measurement data for the rest of the campaign (March 12th to May 2nd, 2024) the correlation is zero.

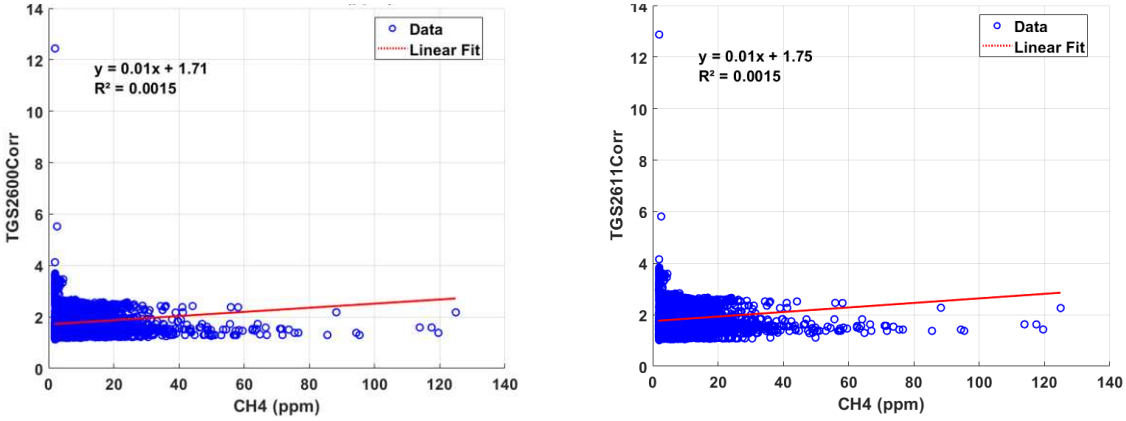

Figure 8: Data used to generate a calibration curve following the methods of Eugster and Kling (2012) for the TGS2600 (left) and the TGS2611 (right). (Rs/R0)corr plotted on the x-axis and methane mixing ratios measured using the Aeris Sentinel on the y-axis.

The sensors were analyzed for cross-sensitivity during the period of deployment. Data from the reference analyzer was used to identify 10-minute periods where the sensors were subject to background methane concentrations before and after deployment. The resistance of the sensors in ambient methane concentrations in relatively constant temperature and humidity (±0.5 °C and ±2 %, respectively) were used to derive a deviation of the signal. Both the TGS2600 and TGS2611 sensors showed low cross-sensitivity indexes of 0.000063 and 0.00027, respectively. Regarding selectivity of gas detection and following the sensors' datasheets, the metal oxide sensors are cross-sensitive to carbon monoxide, iso-butane, ethanol, and hydrogen. However, these gases are unlikely to be a significant source of contamination [30,31,35].

3.2 Machine learning methods

Time series plots of the RF predicted methane concentrations showed a similar pattern to the actual measured concentrations from the Aeris analyzer (Figure 7). The model demonstrated a high sensitivity to the minor variations in input features, enabling noticeable concentration levels with slight changes in sensor and environmental readings. The average measured concentration for the Aeris analyzer (during the measurement period) was 2.40 ppm with a maximum of 147.6 ppm, compared to the average calculated mixing ratios of 2.42 ppm and 2.40 ppm with a maximum value of 117.5 ppm and 106.3 ppm for the TGS2600 and TGS2611, respectively.

The regression analysis for the filtered data yielded significantly improved performance metrics. For the TGS2600, the R^2 value was 0.86, indicating that the model explains 86% of the variance in methane mixing ratios. Similarly, the TGS2611 achieved an R^2 of 0.82, reflecting a strong correlation between the model estimates and the measured concentrations (Figure 8).

The Mean Squared Error (MSE) values were 0.28 for the TGS2600 and 0.35 for the TGS2611, with RMSE values of 0.53 ppm and 0.60 ppm, respectively. These results suggest that the typical prediction errors were substantially reduced. The Mean Absolute Percentage Error (MAPE) values of 3.66% for the TGS2600 and 4.12% for the TGS2611 indicate that the model's predictions were, on average, within approximately 4% of the actual values, demonstrating high accuracy (Table 1).

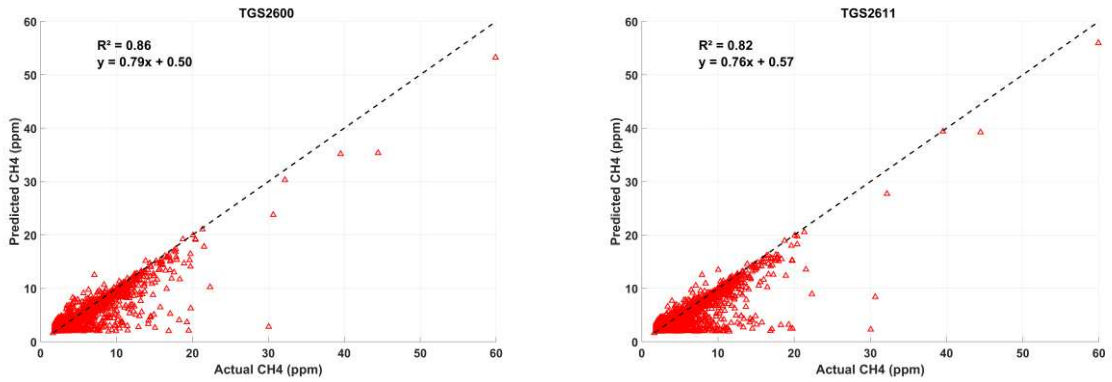

Figure 9: Scatter plots of predicted vs. actual methane concentrations for (left) TGS2600 (R^2 = 0.86, y = 0.79x + 0.50) and (right) TGS2611 (R^2 = 0.82, y = 0.76x + 0.57). The dashed line represents the 1:1 ideal fit.

Table 1: Performance metrics for the mixing ratios generated using the TGS2600 data with the RF algorithm (TGS2600-RF) and mixing ratios generated using the TGS2611 data with the RF algorithm (TGS2611-RF) when compared to measured mixing ratios.

Metric	**TGS2600-RF**	**TGS2611-RF**
R-squared (R^2)	0.86	0.82
Mean Absolute Error (MAE)	0.12	0.14

Mean Squared Error (MSE)	0.28	0.35
Root Mean Squared Error (RMSE)	0.53	0.60
Mean Absolute Percentage Error (MAPE)	3.66%	4.12%
Explained Variance	0.86	0.82

The relative contribution of each feature was also assessed and from these, TGS2600 feature importance scores indicate that the relative humidity feature is the most influential, accounting for approximately 36.1% of the model's predictive power, the sensor resistance at 34.2% and temperature at 29.7%. In the case of the TGS2611, humidity again emerges as the most significant feature, contributing 39.2% to the model's predictions, while the resistance accounts for 33.9% and temperature contributes 26.9% (Figure 10). The consistent significance of humidity across both sensor models suggests its critical role in the accuracy of sensor measurements.

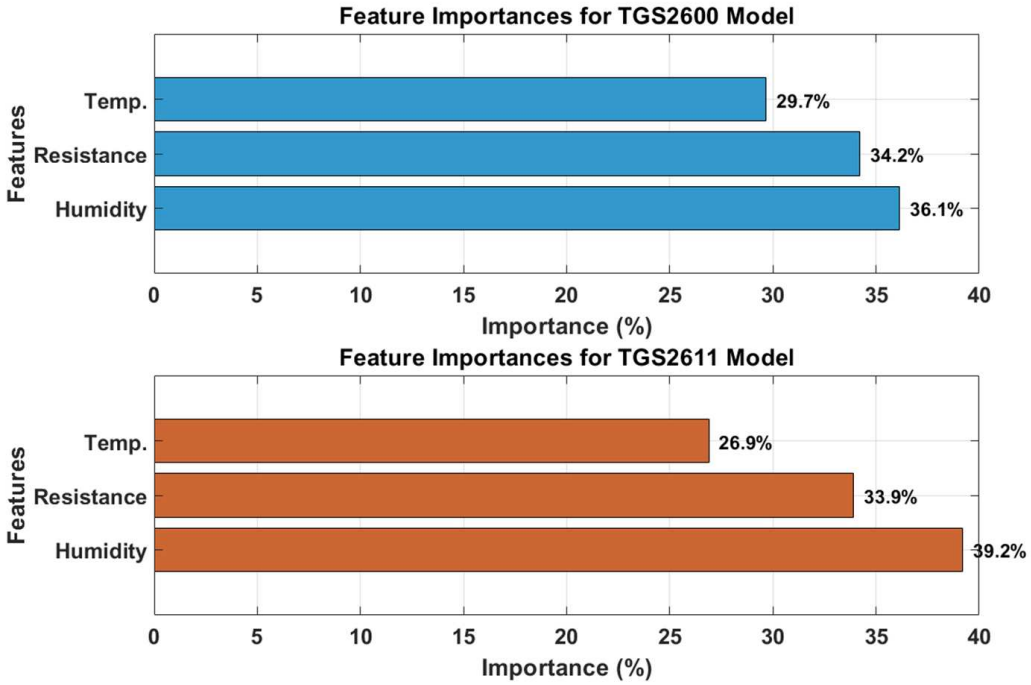

Figure 10: Feature importance analysis of the Random Forest model for methane prediction using TGS2600 (top) and TGS2611 (bottom) sensors. The bars represent the relative contribution of each feature—temperature, resistance, and humidity—to the model's predictive performance.

The model was also tested against the training and test datasets, and it demonstrated strong performance on the training data, with an R-squared value of 0.89 and 0.84 for TGS2600 and TGS2611 respectively. However, the R-squared values on the test data was 0.86 and 0.82, revealing a drop in predictive accuracy when applied to new data. This suggests that the model has become too closely aligned with the specific patterns in the training data, reducing its ability to perform as well on unseen data. This pattern is also evident when new and considerably large datasets with new instances are applied to the model the R-squared value decreases. While the test set performance is still reasonably good, there is room for improvement in enhancing the model's generalizability. Future improvements could be achieved by applying techniques such as

hyperparameter tuning or increasing the size of the training dataset. Additionally, exploring other ensemble models might lead to better overall performance.

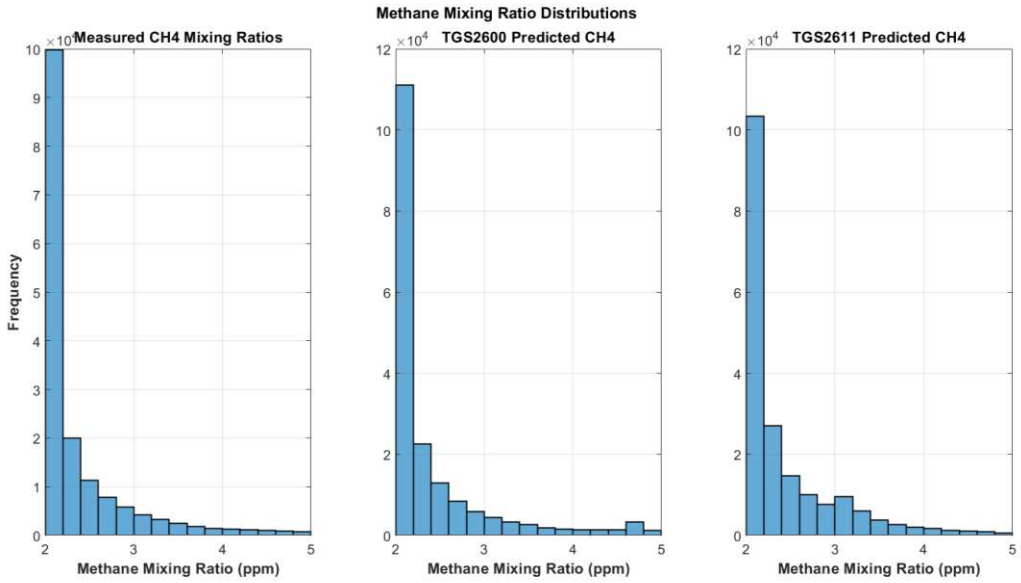

Figure 11: Histograms, comprising of 15 0.2 ppm bins truncated at < 2ppm and >5 ppm, for the measured mixing ratios (left pane), of the mixing ratios calculated using the TGS2600 data with the RF algorithm (center pane) and mixing ratios calculated using the TGS2611 data with the RF algorithm (right pane).

Histograms, comprising of 17 0.2 ppm bins truncated at < 2ppm and >5 ppm (Figure 8), show all data sets are heavily right skewed. Comparisons using the overlap coefficient, also known as Szymkiewicz-Simpson coefficient, show an overlap between the measured mixing ratios and those mixing ratios generated by TGS2600 and TGS2611 of 0.95 and 0.94, respectively. This means that the measured mixing ratios and mixing ratios generated by TGS2600 has 95% of distribution overlapping whereas with TGS2611, it is 94%.

4. DISCUSSION

This study reports the response of two metal oxide sensors, Figaro TGS2600 and TGS2611, to methane emissions at Colorado State University's METEC site between March 1st and May 2nd, 2024. Methane mixing ratios observed by the reference analyzer ranged from background to 119 ppm (Figure 7), while both TGS sensors response showed diurnal variation in response to changes in temperature and relative humidity but no obvious response to changes in methane mixing ratio. When the TGS response data were used to generate calibration curves following published methods [25,30], there was no correlation between the calculated mixing ratios and the measured mixing ratios (Figure 8). A set of training data were then used with the Random Forest machine learning algorithm using the metal oxide sensor resistance, temperature and relative humidity data to map to the measured reference methane mixing ratio data.

4.1 Random Forest calibration versus Linear Regression calibration

The random forest algorithm performed better than the linear regression model. The R^2 for the linear regression model for TGS2600 and TGS2611 are 0.0015 and 0.0015, respectively, compared to the R^2 obtained by the RF model, 0.86 and 0.82, respectively (Table 1). The improvement in R^2 can be attributed to the ability of the RF algorithm to capture non-linear and convoluted interrelations between the sensor outputs and the target variable. In addition, the ability of the RF model to implement bootstrapping and feature randomness reduces the risk of overfitting while allowing the model to popularize better to new datasets. This study also assessed the effect of the

incorporation of larger datasets and advanced techniques such as k-fold cross validation on the model performance. By expanding the model's training dataset, the model better captured the underlying patterns and improved accuracy; however, these improvements often require increased computational power for extensive model evaluation.

4.2 Influence of humidity & temperature

The signal-to-noise ratio of the metal oxide data was too low for previously used calibration methods to be employed. The sensors were deployed through periods of low and high temperatures and humidities. Therefore, the RF algorithm was able to identify the underlying complex relationship between the sensor resistances and the variable conditions that the sensors were exposed to. Humidity was found to be the most influential factor for both sensors, and this could be from formation of a layer of water molecules on the sensing element altering the sensors response. The quality of methane mixing ratio data calculated using the machine learning derived algorithms is similar to those reported previously even though there was a much lower signal-to-noise ratio of input data. Eugster and Kling (2012) reported a R^2 between modeled and measured data between 1.85 and 1.00 ppm of 0.19 [25], for TGS2600 while this study reports an R^2 over the same range of mixing ratios of 0.71. Collier-Oxandale et al. (2018) reported an RMSE of 0.38 for mixing ratios between 2 and 7 ppm [39] for TGS2600, while this study reports an RMSE of 0.18. Riddick et al. (2020a) reported an accuracy of ± 0.01 ppm between 1.85 and 5.85 ppm while this study reports an accuracy of ± 0.24 ppm.

Bastviken et al. (2020) collocated a Figaro NGM2611-E13, which is a calibrated version of TGS2611, with a humidity and temperature sensor in a real-world deployment scenario. They did not explore the interactions between the input variables and used a simpler calibration model with a smaller data set between 619 and 930 datum per sensor, while our study generated 1.6 million data points [40]. Collier-Oxandale et al. (2018) co-located methane sensors with reference instruments during field deployment [39]. Our study used a similar approach only that we used controlled releases in a field setting. The study noted a longer deployment was needed to capture high emission events, which we had control over in our study due to the nature of our releases. Rivera Martinez et al. (2021) calibrated a TGS2611-E00 methane sensor across relatively narrow temperature and humidity ranges (15–30 °C, 40–80%) and 2–9 ppm methane ranges and co-located with an Picarro G2301 Cavity Ringdown Gas Analyzer [41]. They used a linear model whereas our study used the RF algorithm which allows for calibration across a broader range of methane levels. As a result of the varying models used, setup and concentration ranges, it is hard to compare metrics; however, all these studies emphasize the importance of factoring in the humidity and temperature for sensor calibration and the use of a precise reference instrument.

5. CONCLUSIONS

This study provides evidence that machine learning approaches could be used to generate sensor calibration algorithms to better constrain methane mixing ratios measured using low-cost methane sensors. Practically, this would mean that machine learning could be used to derive algorithms to better define complex relationships between sensor outputs and environmental conditions to enable better calibration and improve the metal oxides sensor's accuracy. The main advantages of using machine learning algorithms for generating calibration algorithms is they can model complex relationships between sensor outputs and environmental conditions, and they can reduce the effects of overfitting by using multiple trees. The shortcomings are that with larger datasets, the computational costs increase significantly and that the model interaction between the features are less interpretable as compared to simpler models like linear regression. The development of machine learning algorithms is increasing exponentially, and it is expected that in the future, the model can perform better with less training data while being less affected by noise or sensor anomalies.

This study investigated the use of a machine learning model to calibrate poor quality low-cost, metal oxide sensor data to generate representative methane mixing ratio data. Currently, calibration of metal oxide sensors requires a sensor output with a high signal-to-noise ratio. The high importance of humidity in both TGS2600 and TGS2611 sensors underscores the importance of environmental variability when developing predictive models for gas detection.

Our results also showed that the machine learning derived mixing ratios were as good as those reported by other studies using better signal-to-noise ratio data. While our findings show that machine learning techniques can improve the predictive capabilities of lower-cost sensors such as the TGS2600 and TGS2611 for methane detection, the current performance, with R^2 values of around 0.86 and 0.82, indicates there is still considerable work to be done before these sensors can match the precision and accuracy of high-end trace gas instruments. This would improve low-cost sensors' response, give more confidence to calculated emissions and reduce the uncertainty in greenhouse gas emission inventories.

To further enhance model performance, we explored the impact of increasing computational resources and implementing k-Fold Cross-Validation. Our results confirmed that these adjustments significantly improved the model's predictive capability. By leveraging k-Fold Cross-Validation, we ensured that the model was trained and validated on multiple data subsets, reducing the risk of overfitting and providing a more reliable estimate of its generalization performance. This approach also helped refine the calibration process by better capturing the complex interactions between sensor outputs and environmental conditions.

Additionally, increasing computational resources allowed us to experiment with more complex model architectures and optimize hyperparameters more effectively. The ability to process larger datasets with finer temporal resolutions enabled us to achieve more stable and accurate methane concentration predictions. While low-cost sensors still pose challenges in terms of signal-to-noise ratio and environmental dependencies, these improvements demonstrate the potential of machine

learning-driven calibration to bridge the gap between affordable sensing technologies and high-precision gas analyzers. Future work should focus on integrating additional environmental variables, testing advanced ensemble learning techniques, and optimizing model deployment strategies to further enhance real-world applicability.

APPENDIX

Supplementary Information

a. Confusion matrix for TGS Sensors

i. TGS2600

This matrix compares the predicted methane concentration classes (Low, Medium, High) against the actual classes measured by the Aeris MIRA reference analyzer. The diagonal cells represent correct predictions, with 30,090 correct classifications for the "Low" class and 1 each for the "Medium" and "High" classes. Off-diagonal cells indicate misclassifications, primarily in the "Medium" and "High" ranges. The matrix highlights the TGS2600's strong performance in detecting low methane concentrations but reveals challenges in accurately classifying higher concentrations, likely due to sensor limitations or environmental variability.

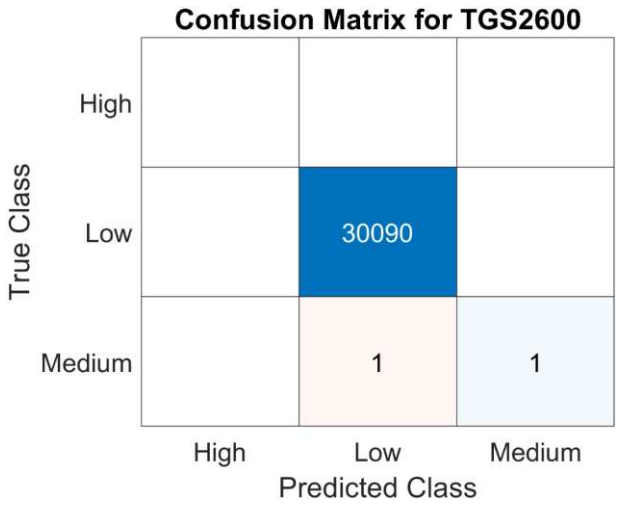

Figure 12: Confusion Matrix for TGS2600

ii. TGS2611

The TGS2611 correctly classified 30,110 instances in the "Low" class and 1 instance in the "Medium" class. Similar to the TGS2600, the sensor struggles with higher concentration classes, as evidenced by the off-diagonal misclassifications. This suggests that while the TGS2611 performs well for low concentrations, its accuracy decreases for medium and high methane levels, possibly due to cross-sensitivity or environmental factors.

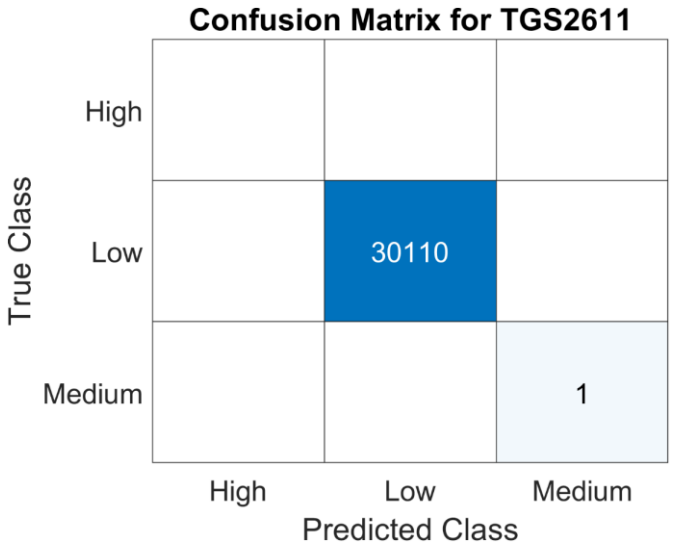

Figure 13: Confusion matrix for TGS2611

b. Error Distribution

i. TGS2600

This histogram shows the frequency of residuals (difference between predicted and actual methane concentrations) for the TGS2600 sensor. The residuals are grouped into bins, with most errors concentrated around 0 ppm. The plot demonstrates that most predictions fall within a small error

range, indicating high accuracy. However, there is a slight tailing of residuals at higher error values, suggesting occasional mispredictions, particularly at higher methane concentrations. This highlights the importance of calibration and environmental correction for improving sensor performance.

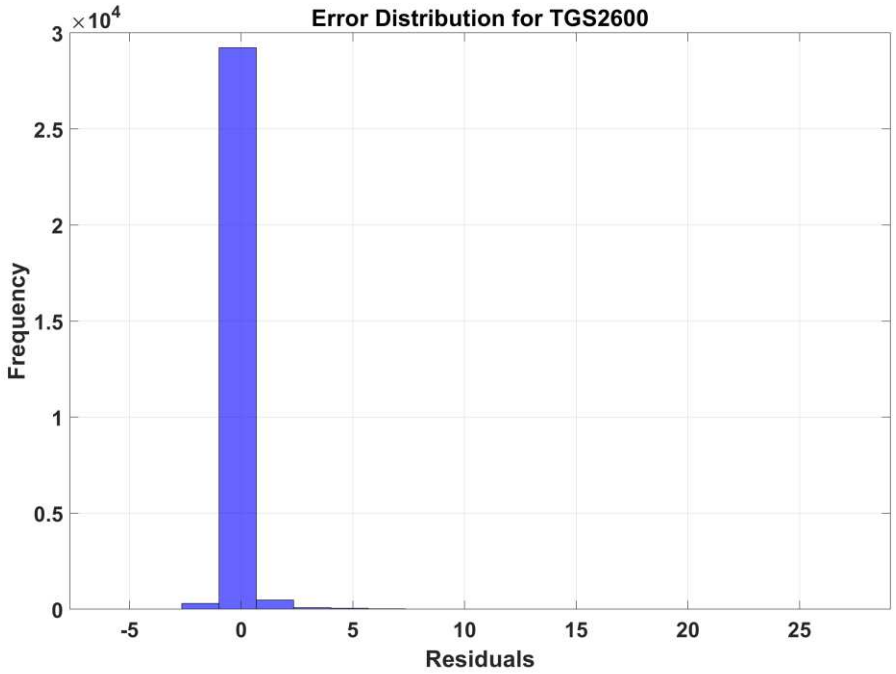

Figure 14: TGS2600 error distribution

ii. TGS2611

Similar to the TGS2600, most errors are concentrated around 0 ppm, indicating high accuracy. However, the TGS2611 shows a slightly wider spread of residuals compared to the TGS2600, particularly in the 10-20 ppm range. This suggests that the TGS2611 is slightly less precise, possibly due to differences in sensor design or sensitivity to environmental factors. The plot

underscores the need for robust calibration methods to minimize errors across all concentration ranges.

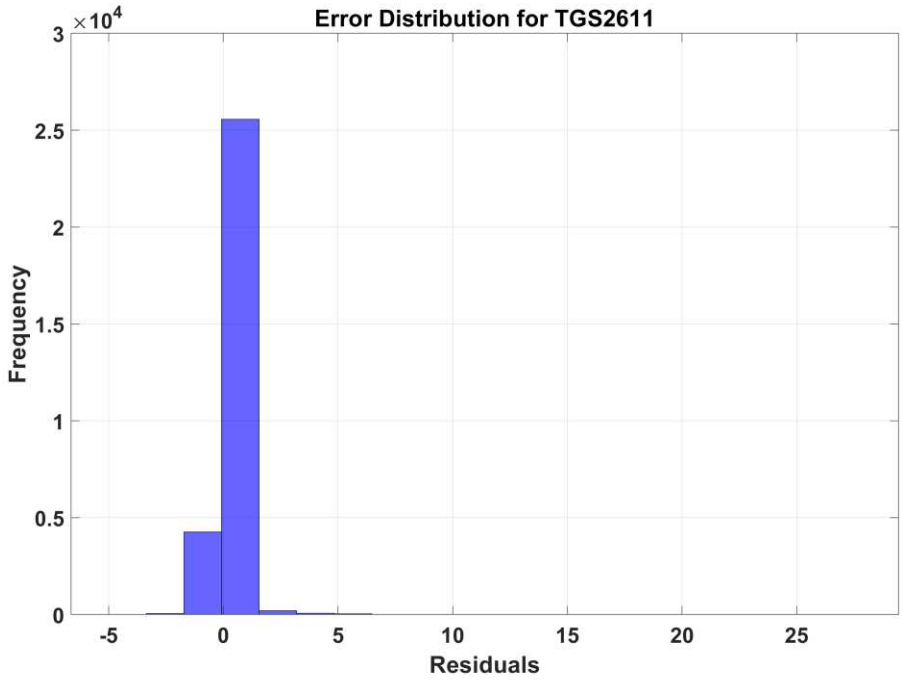

Figure 15: TGS2611 Error Distribution

c. Residuals

i. TGS2611

This plot shows the residuals (difference between predicted and actual methane concentrations) plotted against the predicted concentrations for the TGS2611 sensor. The residuals are clustered around zero, with some deviations at higher concentrations. The plot indicates that the model performs well across most concentration ranges, with errors increasing slightly at higher methane levels. This suggests that while the TGS2611 is generally accurate, it may struggle with high-concentration events, possibly due to sensor saturation or environmental interference. The plot also

highlights the effectiveness of the Random Forest model in reducing systematic errors and improving overall accuracy.

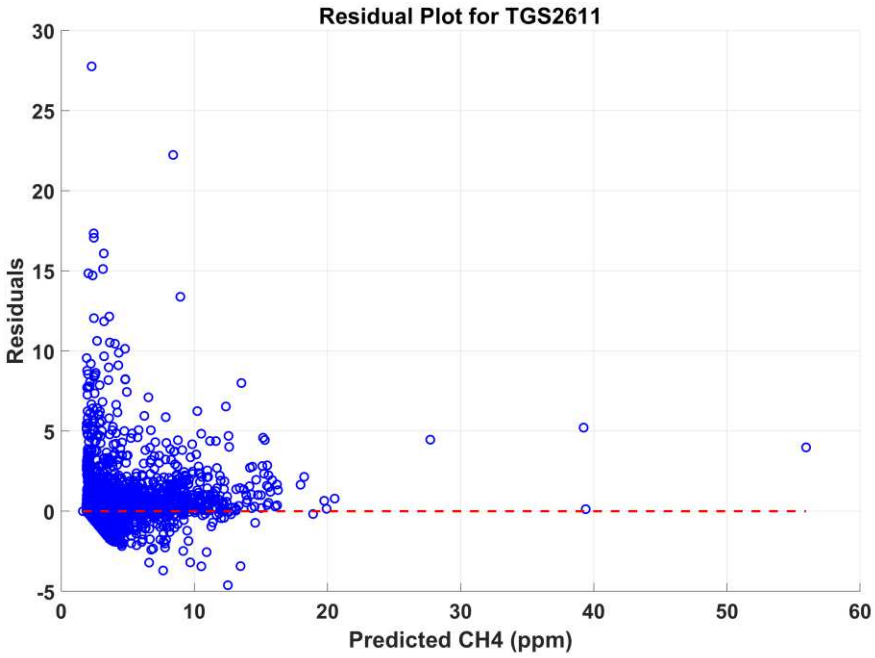

Figure 16: TGS 2611 Residuals

ii. TGS2600

The residuals are tightly clustered around zero, indicating high accuracy across all concentration ranges. The plot demonstrates the effectiveness of the Random Forest model in predicting methane concentrations, with minimal systematic errors. The tight clustering of residuals, even at higher concentrations, suggests that the TGS2600, when calibrated with machine learning, can reliably detect methane across a wide range of conditions.

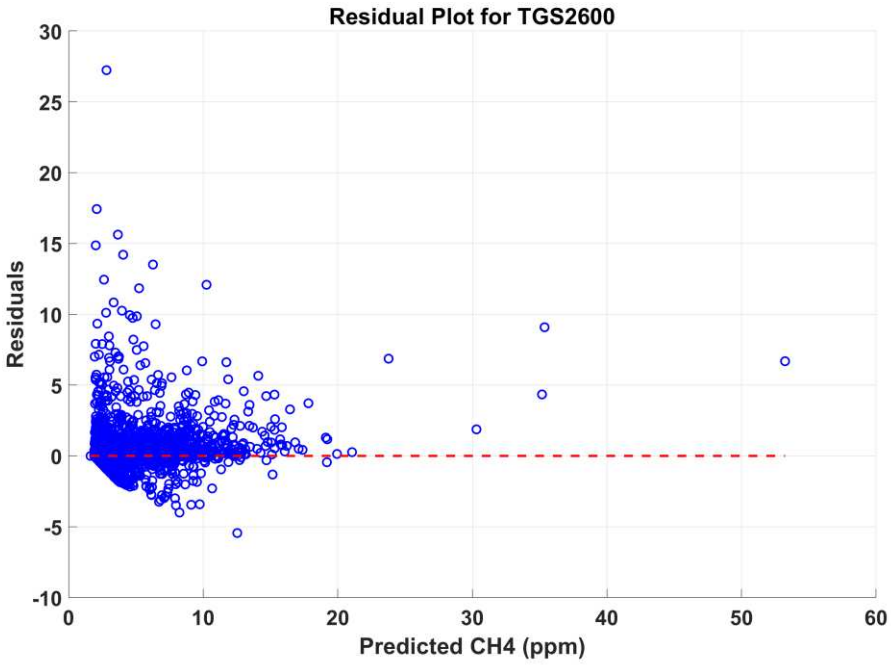

Figure 17: TGS2611 Residuals

REFERENCES

1. IPCC Climate Change 2013 - The Physical Science Basis: Working Group I Contribution to the Fifth Assessment Report of the Intergovernmental Panel on Climate Change; Cambridge University Press: Cambridge, 2014; ISBN 978-1-107-41532-4.

2. IPCC Climate Change 2022: Impacts, Adaptation and Vulnerability. Contribution of Working Group II to the Sixth Assessment Report of the Intergovernmental Panel on Climate Change [H.-O. Pörtner, D.C. Roberts, M. Tignor, E.S. Poloczanska, K. Mintenbeck, A. Alegría, M. Craig, S. Langsdorf, S. Löschke, V. Möller, A. Okem, B. Rama (Eds.)].; Cambridge University Press.: Cambridge University Press, Cambridge, UK and New York, NY, USA, 2022; ISBN 978-1-00-932584-4.

3. Global Methane Pledge Global Methane Pledge - Fast Action on Methane to Keep a 1.5°C Future within Reach Available online: www.globalmethanepledge.org (accessed on 15 September 2022).

4. UNFCCC Paris Agreement. United Nations Framework Convention on Climate Change. FCCC/CP/2015/L.9/Rev.1. Available online: https://unfccc.int/documents/9064 (accessed on 16 June 2023).

5. UNEP/CCAC United Nations Environment Programme and Climate and Clean Air Coalition (2021). Global Methane Assessment: Benefits and Costs of Mitigating Methane Emissions. Nairobi: United Nations Environment Programme. Available online:

https://www.ccacoalition.org/en/resources/global-methane-assessment-full-report (accessed on 25 October 2022).

6. Bell, C.; Ilonze, C.; Duggan, A.; Zimmerle, D. Performance of Continuous Emission Monitoring Solutions under a Single-Blind Controlled Testing Protocol. Environ. Sci. Technol. **2023**, 57, 5794–5805, doi:10.1021/acs.est.2c09235.

7. Caulton, D.R.; Lu, J.M.; Lane, H.M.; Buchholz, B.; Fitts, J.P.; Golston, L.M.; Guo, X.; Li, Q.; McSpiritt, J.; Pan, D.; et al. Importance of Superemitter Natural Gas Well Pads in the Marcellus Shale. Environ. Sci. Technol. **2019**, 53, 4747–4754, doi:10.1021/acs.est.8b06965.

8. Riddick, S.N.; Cheptonui, F.; Yuan, K.; Mbua, M.; Day, R.; Vaughn, T.L.; Duggan, A.; Bennett, K.E.; Zimmerle, D.J. Estimating Regional Methane Emission Factors from Energy and Agricultural Sector Sources Using a Portable Measurement System: Case Study of the Denver–Julesburg Basin. Sensors **2022**, 22, 7410, doi:10.3390/s22197410.

9. Albertson, John.D.; Harvey, T.; Foderaro, G.; Zhu, P.; Zhou, X.; Ferrari, S.; Amin, M.S.; Modrak, M.; Brantley, H.; Thoma, E.D. A Mobile Sensing Approach for Regional Surveillance of Fugitive Methane Emissions in Oil and Gas Production. Environ. Sci. Technol. **2016**, 50, 2487–2497, doi:10.1021/acs.est.5b05059.

10. GRI and EPA Harrison, M.R., Shires, T.M., Wessels, J.K., Cowgill, R. M. Methane Emissions from the Natural Gas Industry, Volumes 1 – 15, Final Report, GRI-94/0257 and EPA-600/R-96- 080, Gas Research Institute and US Environmental Protection Agency, June 1996. **1996**.

11. Campbell, L.M.; Campbell, M.V.; Epperson, D.L. Methane Emissions from the Natural Gas Industry, Volume 2: Technical Report, Final Report, GRI-94/0257.1 and EPA-600/R-96-080b. Gas Research Institute and U.S. Environmental Protection Agency. **1996**.

12. Riddick, S.N.; Mauzerall, D.L. Likely Substantial Underestimation of Reported Methane Emissions from United Kingdom Upstream Oil and Gas Activities. Energy Environ. Sci. **2023**, 16, 295–304, doi:10.1039/D2EE03072A.

13. Caulton, D.R.; Li, Q.; Bou-Zeid, E.; Fitts, J.P.; Golston, L.M.; Pan, D.; Lu, J.; Lane, H.M.; Buchholz, B.; Guo, X.; et al. Quantifying Uncertainties from Mobile-Laboratory-Derived Emissions of Well Pads Using Inverse Gaussian Methods. Atmospheric Chem. Phys. **2018**, 18, 15145–15168, doi:10.5194/acp-18-15145-2018.

14. Peischl, J.; Eilerman, S.J.; Neuman, J.A.; Aikin, K.C.; de Gouw, J.; Gilman, J.B.; Herndon, S.C.; Nadkarni, R.; Trainer, M.; Warneke, C.; et al. Quantifying Methane and Ethane Emissions to the Atmosphere From Central and Western U.S. Oil and Natural Gas Production Regions. J. Geophys. Res. Atmospheres **2018**, doi:10.1029/2018JD028622.

15. Pétron, G.; Karion, A.; Sweeney, C.; Miller, B.R.; Montzka, S.A.; Frost, G.J.; Trainer, M.; Tans, P.; Andrews, A.; Kofler, J.; et al. A New Look at Methane and Nonmethane Hydrocarbon Emissions from Oil and Natural Gas Operations in the Colorado Denver-Julesburg Basin. J. Geophys. Res. Atmospheres **2014**, 119, 6836–6852, doi:10.1002/2013JD021272.

16. Barkley, Z.; Davis, K.; Miles, N.; Richardson, S.; Deng, A.; Hmiel, B.; Lyon, D.; Lauvaux, T. Quantification of Oil and Gas Methane Emissions in the Delaware and Marcellus Basins Using

a Network of Continuous Tower-Based Measurements. Atmospheric Chem. Phys. **2023**, 23, 6127–6144, doi:10.5194/acp-23-6127-2023.

17. Riddick, S.N.; Ancona, R.; Cheptonui, F.; Bell, C.S.; Duggan, A.; Bennett, K.E.; Zimmerle, D.J. A Cautionary Report of Calculating Methane Emissions Using Low-Cost Fence-Line Sensors. Elem. Sci. Anthr. **2022**, 10, 00021, doi:10.1525/elementa.2022.00021.

18. Cho, Y.; Smits, K.M.; Riddick, S.N.; Zimmerle, D.J. Calibration and Field Deployment of Low-Cost Sensor Network to Monitor Underground Pipeline Leakage. Sens. Actuators B Chem. **2022**, 355, 131276, doi:10.1016/j.snb.2021.131276.

19. Vaughn, T.L.; Bell, C.S.; Pickering, C.K.; Schwietzke, S.; Heath, G.A.; Pétron, G.; Zimmerle, D.J.; Schnell, R.C.; Nummedal, D. Temporal Variability Largely Explains Top-down/Bottom-up Difference in Methane Emission Estimates from a Natural Gas Production Region. Proc. Natl. Acad. Sci. **2018**, 115, 11712–11717, doi:10.1073/pnas.1805687115.

20. Riddick, S.N.; Mbua, M.; Santos, A.; Hartzell, W.; Zimmerle, D.J. Potential Underestimate in Reported Bottom-up Methane Emissions from Oil and Gas Operations in the Delaware Basin. Atmosphere **2024**, 15, 202, doi:10.3390/atmos15020202.

21. Bell, C.S.; Vaughn, T.L.; Zimmerle, D.; Herndon, S.C.; Yacovitch, T.I.; Heath, G.A.; Pétron, G.; Edie, R.; Field, R.A.; Murphy, S.M.; et al. Comparison of Methane Emission Estimates from Multiple Measurement Techniques at Natural Gas Production Pads. Elem Sci Anth **2017**, 5, 79, doi:10.1525/elementa.266.

22. Bell, C.; Rutherford, J.; Brandt, A.; Sherwin, E.; Vaughn, T.; Zimmerle, D. Single-Blind Determination of Methane Detection Limits and Quantification Accuracy Using Aircraft-Based LiDAR. Elem. Sci. Anthr. **2022**, 10, 00080, doi:10.1525/elementa.2022.00080.

23. Shah, A.; Laurent, O.; Lienhardt, L.; Broquet, G.; Rivera Martinez, R.; Allegrini, E.; Ciais, P. Characterising the Methane Gas and Environmental Response of the Figaro Taguchi Gas Sensor (TGS) 2611-E00. Atmospheric Meas. Tech. **2023**, 16, 3391–3419, doi:10.5194/amt-16-3391-2023.

24. Shah, A.; Laurent, O.; Broquet, G.; Philippon, C.; Kumar, P.; Allegrini, E.; Ciais, P. Determining Methane Mole Fraction at a Landfill Site Using the Figaro Taguchi Gas Sensor 2611-C00 and Wind Direction Measurements. Environ. Sci. Atmospheres **2024**, 4, 362–386, doi:10.1039/D3EA00138E.

25. Eugster, W.; Kling, G.W. Performance of a Low-Cost Methane Sensor for Ambient Concentration Measurements in Preliminary Studies. Atmospheric Meas. Tech. **2012**, 5, 1925–1934, doi:10.5194/amt-5-1925-2012.

26. Eugster, W.; Laundre, J.; Eugster, J.; Kling, G.W. Long-Term Reliability of the Figaro TGS 2600 Solid-State Methane Sensor under Low-Arctic Conditions at Toolik Lake, Alaska. Atmospheric Meas. Tech. **2020**, 13, 2681–2695, doi:10.5194/amt-13-2681-2020.

27. Lin, J.J.Y.; Buehler, C.; Datta, A.; Gentner, D.R.; Koehler, K.; Zamora, M.L. Laboratory and Field Evaluation of a Low-Cost Methane Sensor and Key Environmental Factors for Sensor Calibration. Environ. Sci. Atmospheres **2023**, 3, 683–694, doi:10.1039/D2EA00100D.

28. Nagahage, I.S.P.; Nagahage, E.A.A.D.; Fujino, T. Assessment of the Applicability of a Low-Cost Sensor–Based Methane Monitoring System for Continuous Multi-Channel Sampling. Environ. Monit. Assess. **2021**, 193, 509, doi:10.1007/s10661-021-09290-w.

29. Sugriwan, I.; Soesanto, O. Development of TGS2611 Methane Sensor and SHT11 Humidity and Temperature Sensor for Measuring Greenhouse Gas on Peatlands in South Kalimantan, Indonesia. J. Phys. Conf. Ser. **2017**, 853, 012006, doi:10.1088/1742-6596/853/1/012006.

30. Riddick, S.N.; Mauzerall, D.L.; Celia, M.; Allen, G.; Pitt, J.; Kang, M.; Riddick, J.C. The Calibration and Deployment of a Low-Cost Methane Sensor. Atmos. Environ. **2020**, 230, 117440, doi:10.1016/j.atmosenv.2020.117440.

31. Figaro Production Information. TGS 2611 - for the Detection of Methane. Https://Www.Figarosensor.Com/Product/Docs/TGS%202611C00(1013).Pdf. Last Accessed 8/26/21. 2020.

32. Andrews, B.; Chakrabarti, A.; Dauphin, M.; Speck, A. Application of Machine Learning for Calibrating Gas Sensors for Methane Emissions Monitoring. Sensors **2023**, 23, 9898, doi:10.3390/s23249898.

33. Breiman, L. Random Forests. Mach. Learn. **2001**, 45, 5–32, doi:10.1023/A:1010933404324.

34. MIRA Mobile Methane/Ethane Analyzers. Aeris Technol.

35. Tgs2600_product_information_rev02.Pdf.

36. Han, S.; Kim, H. Optimal Feature Set Size in Random Forest Regression. Appl. Sci. **2021**, 11, 3428, doi:10.3390/app11083428.

37. Ellis, C. Hyperparameter Tuning in Random Forests Available online: https://crunchingthedata.com/hyperparameter-tuning-in-random-forests/ (accessed on 13 August 2024).

38. Furuta, D.; Sayahi, T.; Li, J.; Wilson, B.; Presto, A.A.; Li, J. Characterization of Inexpensive Metal Oxide Sensor Performance for Trace Methane Detection. Atmospheric Meas. Tech. **2022**, 15, 5117–5128, doi:10.5194/amt-15-5117-2022.

39. Collier-Oxandale, A.; Casey, J.G.; Piedrahita, R.; Ortega, J.; Halliday, H.; Johnston, J.; Hannigan, M.P. Assessing a Low-Cost Methane Sensor Quantification System for Use in Complex Rural and Urban Environments. Atmospheric Meas. Tech. **2018**, 11, 3569–3594, doi:10.5194/amt-11-3569-2018.

40. Bastviken, D.; Nygren, J.; Schenk, J.; Parellada Massana, R.; Duc, N.T. Technical Note: Facilitating the Use of Low-Cost Methane (CH_4) Sensors in Flux Chambers – Calibration, Data Processing, and an Open-Source Make-It-Yourself Logger. Biogeosciences **2020**, 17, 3659–3667, doi:10.5194/bg-17-3659-2020.

41. Rivera Martinez, R.; Santaren, D.; Laurent, O.; Cropley, F.; Mallet, C.; Ramonet, M.; Caldow, C.; Rivier, L.; Broquet, G.; Bouchet, C.; et al. The Potential of Low-Cost Tin-Oxide Sensors Combined with Machine Learning for Estimating Atmospheric CH4 Variations around Background Concentration. Atmosphere **2021**, 12, 107, doi:10.3390/atmos12010107.